MAGMA (1994) 2, 79–89

A time-efficient method for combined T_1 and T_2 measurement in magnetic resonance imaging: Evaluation for multiparameter tissue characterization

Manfred Eis and Mathias Hoehn-Berlage*

Department of Experimental Neurology, Max-Planck-Institute for Neurological Research, Köln, Germany

A new magnetic resonance imaging high-resolution sequence is presented that allows for the collection of all data for determination of T_1 and ρ as well as for multiexponential T_2 analysis within one measurement cycle.

Noise preprocessing is performed in order to avoid systematic errors in relaxation parameter analysis and to increase the interexperimental reproducibility of the results. For T_2 analysis, an optimized Marquardt algorithm is used, in combination with image processing methods for both automatic detection of voxels with partial volume effects, and for speedup of the iterative nonlinear regression steps. Determination of longitudinal relaxation time is based on a sophisticated signal intensity ratio technique that computes T_1 as the mean of up to eight individual T_1 values, each weighted with its relative T_2 decay. Relative proton density is computed using results of the evaluations of both relaxation times. Validation of the method is accomplished by comparing phantom measurements with reference data acquired with spectroscopic sequences. *In vivo* examples of the computed parameter images taken from a study of experimental cerebral infarcts in rats are presented.

The method allows one to acquire high-resolution parameter images within a measurement time that is tolerable even in clinical routine. Furthermore, the chosen evaluation concepts guarantee a short computation time. Therefore, an on-line computation of the parameter images and, in consequence, their direct use for diagnostic purposes appears feasible.

Keywords: MR imaging, relaxation times, proton density, double delay multiecho, high resolution parameter images, tissue characterization.

INTRODUCTION

In 1971 Damadian [1] observed a distinct difference in T_1 proton relaxation time between normal and cancerous tissues. Therefore, the application of relaxation measurements for diagnostic purposes gained much attention, leading to a large number of relaxation studies on *in vitro* tissue specimens. In a high number of cases, these investigations showed reliable tissue discrimination based on T_1 and/or T_2 relaxation time values (for comprehensive reviews, see Refs. 2–4).

Address for correspondence: Max-Planck-Institut für neurologische Forschung, Abteilung für experimentelle Neurologie, D-50931 Köln, Germany.

Received 28 November 1993 and in revised form 28 January 1994.

Clinical diagnosis with magnetic resonance imaging (MRI) relies on T_1-, T_2- and proton-density-weighted images expressing changes in parameters only in a *qualitative* way. Therefore, the successful *in vitro* tissue discrimination with MR relaxometry motivated several scientists to measure relaxation times and proton density *in vivo* in order to obtain a set of physical parameters for a *quantitative* tissue description, which considerably expands the potentials of MRI.

In order to optimize this tissue characterization approach, as many parameters as possible must be measured with both high precision and reproducibility. There is also a need to preserve high spatial resolution without compromising measurement time. Most previous studies have used multiecho experiments for assessment of transversal relaxation parameters [5–9], and standard saturation recovery (SR)

[10–12], inversion recovery (IR) [13, 14], mixed SR/IR [15–17], IR multiecho [18] or multipoint partial saturation [8] methods for measurement of T_1. These time-consuming approaches can be sped up by the use of one-shot versions of the standard methods [19–21]. Alternatively, if reduced spatial resolution is acceptable, high-speed sequences such as IR Snapshot FLASH (Fast Low Angle Shot) [22–24] and Look-Locker-EPI (Echo Planar Imaging) [25, 26] have been used. Recently, even the acquisition of high-resolution images using Snapshot FLASH has been reported [27]. Nevertheless, so far only very few reports exist on methods allowing the measurement of both relaxation times using just one single sequence [6, 7, 18, 28, 29].

Here we describe the development of an imaging pulse sequence allowing the combination of seemingly opposing requirements: high-resolution quantitative images of T_1, the proton density ρ, multiexponentially analyzed T_2, a measurement time that is tolerable even in the clinical routine, and full practical versatility (e.g., multislice imaging, oblique slices, no special adjustment procedures). For multiexponential T_2 relaxation analysis, Marquardt's algorithm [30] was modified and combined with image processing methods for both automatic detection of partial volume voxels and speedup of the iterative nonlinear regression steps [31, 32]. A known formalism for the description of echo signal amplitudes of multiecho trains [33] was adapted to the specific conditions of our sequence (two echo trains). Using this formalism and information available from the T_2 analysis, an extremely fast algorithm for precise and robust determination of T_1 and ρ [29] was applied. For validation, a relaxation phantom was designed and measured exactly with spectroscopic standard methods. Extensive phantom measurements were carried out with the imaging sequence and compared with the reference data.

For demonstration of the quality of the resulting parameter images, *in vivo* examples from studies of experimental cerebral infarcts in rats are presented.

MATERIALS AND METHODS

Imaging sequence

For measurement of both T_1 and T_2, a Carr–Purcell–Meiboom–Gill (CPMG) [34–36] multislice multiecho sequence was modified [37, 38] and implemented on a Bruker Biospec (Bruker, Karlsruhe, Germany) operating at an induction field of 4.7 T. Basically, the sequence consisted of a first train of 32 echoes acquired after a long recovery time (typically, $TR_1 = 3000$ ms; $\Delta TE = 12.7$ ms), followed by a second excitation to obtain a second train of 8 echoes with a short TR time (typically, $TR_2 = 600$ ms) for each phase-encoding step (Fig. 1). Strong, constant spoiler gradients were applied along the slice selection direction in order to destroy transverse magnetization components remaining after the last echo of each train. Radio frequency (RF) inhomogeneities of the refocusing pulses were accounted for by a two-phase-cycling scheme (0°, 180°) for the two excitation pulses. This phase cycle corresponded to an inherent twofold signal averaging and, hence, resulted in a good signal-to-noise ratio (S/N). Several gradient points (four for slice selection and read-out, each) were experimentally optimized using the standard multiecho version of the sequence and a cubic water phantom, while applying image parameters (field of view, slice thickness, slice–slice distance) typically used for *in vivo* studies. First, the trim points of the read gradient were adjusted for both miminization of stimulated echoes and maximization of first, second, and third (representative for all consecutive ones) echo amplitudes. Additionally, phases of these echoes were intended to be near or equal zero. Afterward, with these read gradients, slice gradients were optimized, measuring independently the first, second, and third echo of eight simultaneously acquired slices. The optimization procedure aimed at highly uniform signal intensities and echo decays over eight slices, independently of the slice position as long as the distance to isocenter of the magnet was below 2 cm.

Multiexponential T_2 analysis was performed on the basis of the 32 echoes of the first echo train. T_1 was determined from signal intensity ratios of the corresponding first eight echoes of each echo train. The results of both evaluation stages were utilized to compute the proton density ρ.

Phantom measurements

In order to test the proposed method under conditions comparable to the *in vivo* situation, 16 different mixtures of H_2O, D_2O, agarose and $NiCl_2$ served as phantom substances mimicking the relaxation behavior of biological tissues [39] at the available field strength.

For the MRI studies with the sequence described above, an actively shielded gradient insert (maximum gradient strength 100 mT/m; rise time <250 μs) and a homogeneous Alderman–Grant ^{1}H-resonator were used. To determine the dependence of the evaluated relaxation parameter values on S/N, RF inhomogeneity, field of view and slice thickness, extensive measurements and simulations were carried out [37]. These results as well as an algorithm to correct for diffusion effects in relaxation time measurements will be reported elsewhere (Eis and Hoehn-Berlage, manuscript

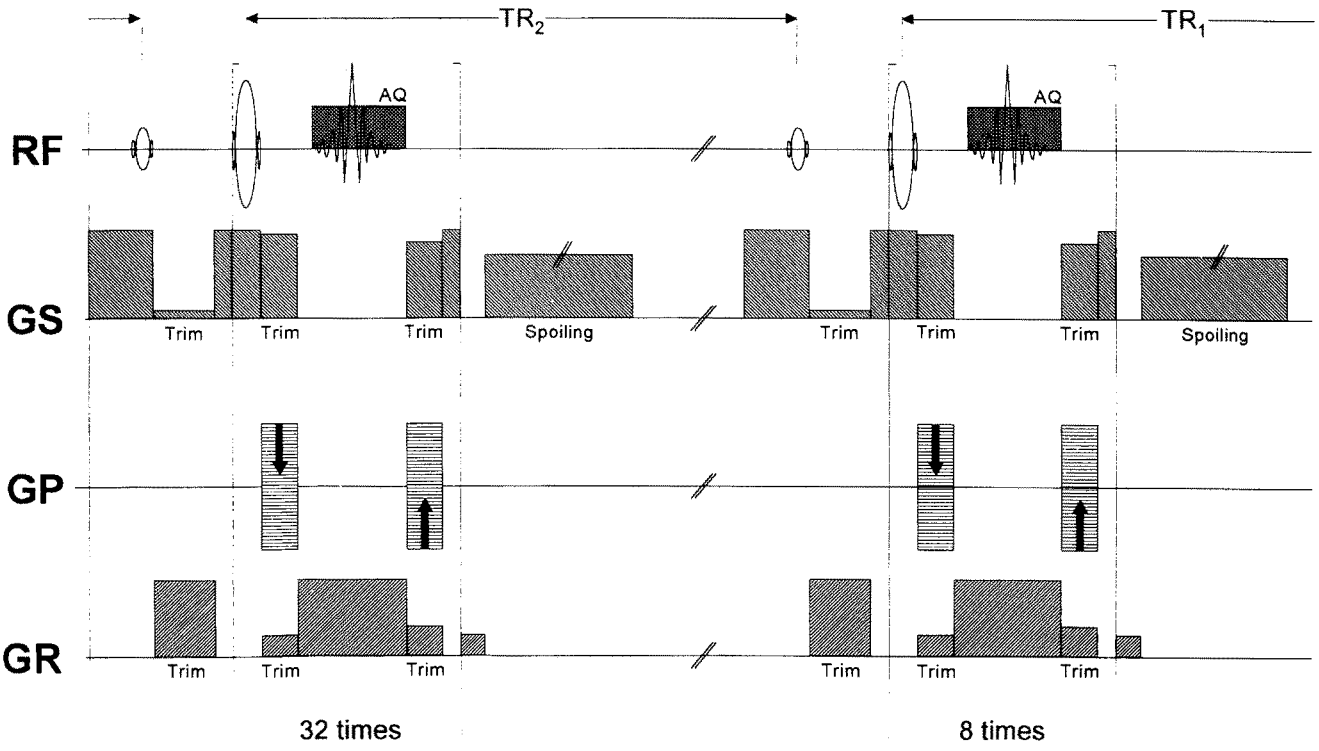

Fig. 1. Correctly scaled pulse scheme of the multislice multiecho pulse sequence used for relaxometry studies. The sequence consists of 2 echo trains (32 and 8 echoes, respectively) recorded with different recovery times $TR_{1/2}$ and identical echo delays ΔTE = 12.7 ms. The two recovery times are defined as the interval between the center of the last refocusing pulse of the first (second) echo train and the excitation pulse of the second (first) train. Therefore, the time available for longitudinal recovery equals the total time without RF irradiation. (RF: radio frequency pulses and echo signal; AQ: aquisition of echo; GS: slice selection gradients; GP: phase-encoding gradients; GR: read-out gradients; Trim: gradient points to be optimized for maximal echo signal; Spoiling: crusher gradients to destroy residual transversal magnetization before the next excitation pulse is transmitted.)

in preparation). To judge the typical accuracy of the method, the 16 vials of phantom substances were measured in two groups of 8 vials each, using the following fixed sequence parameters: TR_1 = 4000 ms, TR_2 = 700 ms, field of view 5.0 cm, slice thickness 10 mm, two signal averagings, image matrix 128 × 256.

Reference data for T_1 and T_2 were determined spectroscopically on our Biospec system, thus eliminating any dependence of the results on the magnet or RF hardware.

For spectroscopic T_2 analysis, 100 echoes were acquired with a CPMG multiecho sequence. In order to avoid spin locking effects due to extremely short echo times [40] and to record the same decay interval covered in the imaging sequence, TE = 4.0 ms was chosen as equidistant read-out delay. The processing steps of each spectrum (containing only a single line) were baseline correction, Fourier transform, magnitude calculation and peak picking. RF pulses were nonselective. To account for eventual RF inhomogeneities, a 4-phase-cycling scheme was applied. S/N was maximized by 16 signal averages (every phase-cycle fourfold). Noisy data points were excluded from the regression analysis. The influence of diffusion was found to be negligible: knowing both the field inhomogeniety over the probe diameter from determination of the line widths and the diffusion coefficients of the phantom substances (which were measured in parallel), attenuation of the last echo due to diffusion was calculated to be lower than 10^{-5} [37].

T_1 measurements were carried out using a spectroscopic IR sequence, again using nonselective RF pulses. Recovery time amounted to at least $5T_1$; inversion time TI was varied nonequidistantly between 10 ms and 10 s, yielding 28 data points. Spectra were processed identically with the CPMG measurements. To determine the longitudinal relaxation time from the spectroscopic IR data, the three free parameters of the model

$$S(\mathrm{TI}) = \left| A - B \cdot \exp\left(-\frac{\mathrm{TI}}{T_1}\right)\right| \qquad (1)$$

were fitted to the data points applying a least squares criterion. Nonlinear regression analysis algorithms

were provided by the CERN software package MINUIT [41] (commands Seek, Simplex, Minimize, Improve, Minos).

ρ values resulted from the known mixture ratios.

Data analysis

Data preprocessing: analysis of image background noise

It is well known that in MRI not only electronically induced noise is present [42, 43]. Additionally, patient-related noise sources like thermally generated, randomly fluctuating noise currents in the body also affect image quality. Referring to the two-dimensional Fourier transform (2DFT), noise is distributed uniformly throughout the reconstructed images [42] and can, therefore, be observed even in the object-free background of the image [44, 45]. Furthermore, even very slight patient motions during the acquisition of the raw data or flow effects result in phase errors, which induce a band of higher noise values in the phase-encoding direction [43]. Due to the magnitude calculation $S = \sqrt{S_R^2 + S_I^2}$, applied to the real part S_R and the imaginary part S_I after 2DFT of the measured complex signal, each pixel signal S in the image background is always greater than zero [31, 44, 45].

In the case of a multiecho sequence, this results in echo trains approaching a positive baseline although the underlying T_2 relaxation process causes an asymptotic signal decay, i.e., leads to zero intensity at very long TE times. As a consequence, artificially long T_2 components were evaluated if the background noise was not taken into consideration before multiexponential T_2 analysis [31, 46]. For the proposed T_1 evaluation scheme, signal intensity ratios computed from noisy data as well as such overestimation of T_2 also led to erroneous results. We, therefore, used an algorithm for noise preprocessing [31, 46] that computed mean m_m and standard deviation σ_m of the background noise for each of the 40 echo images in a quick and completely automatic fashion. The image-specific noise limits NL_m were defined as

$$NL_m = m_m + 3\sigma_m \quad (m = 1, \ldots, 40) \tag{2}$$

Only the signals of the first M pixels that lie above their noise limit NL_m were used for pixelwise evaluation of the relaxation parameters. Considering the changing noise levels within a multiecho image sequence by use of echo-specific noise limits, the maximum number of reliable data points was available for multiexponential T_2 analysis. In general, systematically wrong T_2 and T_1 values due to noise were avoided. As an additional benefit, interexperimental variations of the evaluated relaxation parameters were reduced significantly (Eis, Handels, and Hoehn-Berlage, manuscript in preparation).

Multiexponential T_2 analysis

In view of the very few reports on longitudinal multiexponentiality [47–50], monoexponential T_1 relaxation was assumed. Furthermore, neglecting microcirculation (diffusion, perfusion), flow and saturation effects due to the high number of transmitted RF pulses, the signal equation for a multiecho train is given by

$$S(TR_i, TE_j) = c\rho\left[1 - \exp\left(-\frac{TR_i}{T_1}\right)\right] \cdot \sum_{k=1}^{K} \alpha_k \exp\left(\frac{TE_j}{T_{2_k}}\right) \quad (i = 1, 2;\ j = 1, \ldots, 32) \tag{3}$$

where c denotes an image scaling constant, ρ the total proton density, and $\alpha_k (\sum_{k=1}^{K} \alpha_k = 1)$ the relative contribution of each relaxing component k (K in total) present within the voxel. Referring to our imaging sequence, the first echo train, consisting of 32 echoes, was used for T_2 analysis and, hence, TR_i was equivalent to the long recovery time TR_1. Defining S_{0_k} as the signal strength of each compartment at echo time TE = 0

$$S_{0_k} \equiv S(TR_1, TE = 0) = c\rho\alpha_k\left[1 - \exp\left(-\frac{TR_1}{T_1}\right)\right] \tag{4}$$

the equation used for multiexponential T_2 analysis simplifies as follows:

$$S(TE_j) = \sum_{k=1}^{K} S_{0_k} \exp\left(-\frac{TE_j}{T_{2_k}}\right). \tag{5}$$

The relaxation parameters S_{0_k} and T_{2_k} of each compartment were evaluated using a modification of the Marquardt algorithm [30–32].

As there is great variety in compartmentation and molecular structure of tissues, multiexponential T_2 relaxation behavior is a structural property of some tissues (e.g., fat and bone marrow) and, hence, a tissue characteristic feature [5, 7, 9, 31, 51–54]. In MRI, an additional kind of multiexponentiality is observed that is due to mixtures of different tissues contained in one voxel (partial volume effects). According to the principle of superposition, monoexponential decay curves from different compartments within a volume element result in experimentally observable multiexponential characteristics of the corresponding pixel. Evidently, calculation of relaxation parameters without the exclusion of partial volume voxels leads to errone-

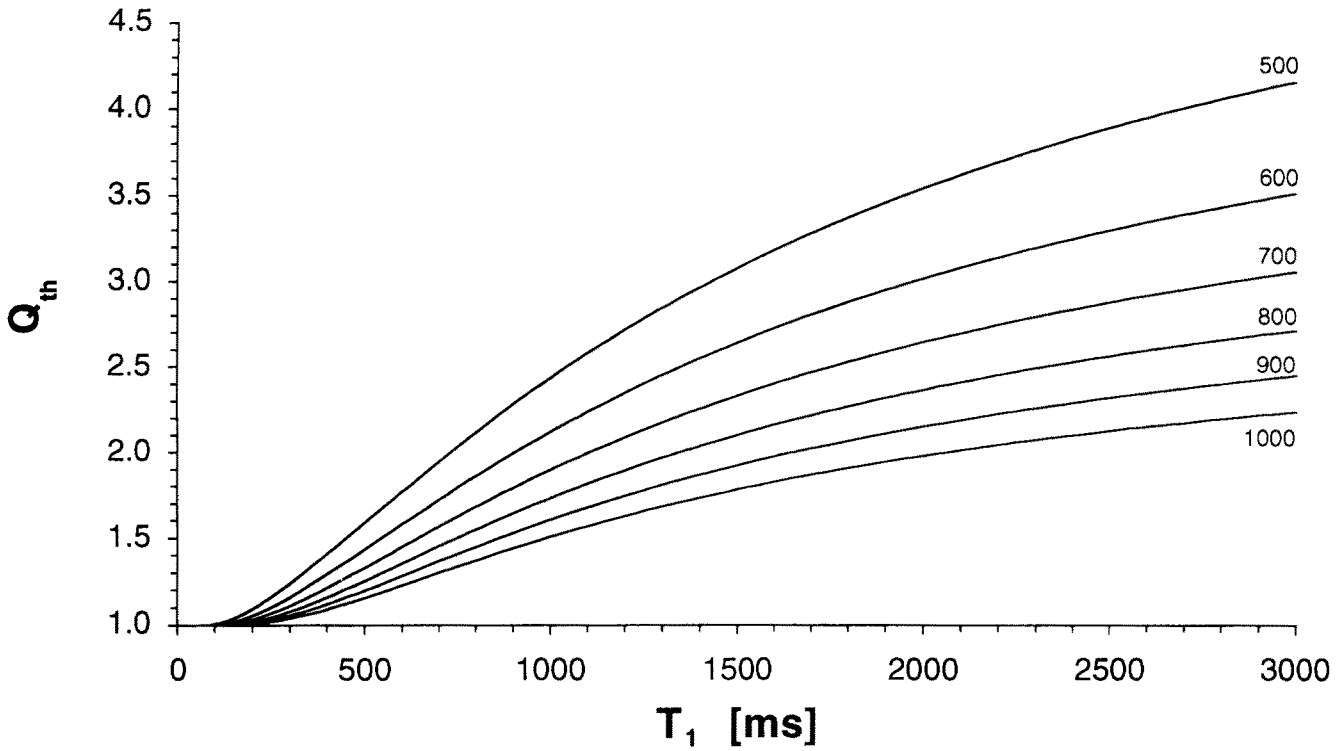

Fig. 2. Theoretical signal ratio Q_{th} as a function of T_1 for a given TR_1 of 3000 ms and several TR_2 times (data are indicated on curves; in ms). Note that an extremely inadequate combination of the two recovery times will lead to a nonunambiguous behavior of Q_{th}, thus making the bisection method for scanning of the LUT impossible.

ous results, which cannot be regarded as tissue-characteristic.

In order to distinguish these two types of multiexponentially relaxing voxels, we used an image processing algorithm developed by Handels *et al.* [31, 32]: Tissue boundary regions were characterized by regionally high T_2 variations and detected automatically analyzing the (3 × 3)-neighborhood of the actually evaluated pixel. Using this algorithm, partial-volume effects both in plane and perpendicular to the imaging slice could be detected, because the partial-volume mixing of different contributing structures is independent of their respective position within the voxel under consideration. Furthermore, optimal starting values for speedup of the iterative nonlinear regression steps were found using the multiexponential results of the upper and left neighbor pixels.

Determination of T_1 and relative proton density ρ

In order to take the effects of longitudinal relaxation during interpulse delays into account, an already described mathematical formalism [33] for the description of multiecho experiments was adapted to the analysis of our echo sequence [37, 38]. Assuming perfect RF homogeneity, Eq. (3) had to be modified by the saturation recovery correction factors f_{SR_i} for the two multiecho trains:

$$f_{SR_i} = \exp\left(\frac{\tau}{T_1}\right) \cdot \frac{1 + \exp\left[-2N_{i\pm1}(\tau/T_1)\right][\cosh(\tau/T_1) - 1]}{\cosh(\tau/T_1)} \quad (i = 1, 2) \tag{6}$$

where τ = TE/2 and $N_{i\pm1}$ denotes the total number of echoes of the other train, i.e., $N_2 = 8$ for f_{SR_1} and $N_1 = 32$ for f_{SR_2}, respectively. Defining the ratio Q_{th} of the signal intensites of both echo trains ($i = 1, 2$) at arbitrary echo time TE

$$Q_{th}(T_1) \equiv \frac{S(TR_1, TE_j)}{S(TR_2, TE_j)} = \frac{1 - f_{SR_1}\exp(-TR_1/T_1)}{1 - f_{SR_2}\exp(-TR_2/T_1)} \tag{7}$$

the (multiexponential) T_2 dependence of the echo signals was eliminated from the T_1 calculation. For each evaluation of an entire T_1 parameter image, the theoretical ratio Q_{th} was computed once for the actual TR values and all T_1 between 30 and 3000 ms (step width 1 ms) and stored in a look-up table (LUT). The influence of varying TR_2 for a given TR_1 on the Q_{th} function is illustrated in Fig. 2.

In practice, at first all relevant signals (echoes 1–8 and 33–40, respectively) were subjected to the noise preprocessing described above and the number J of echo pairs (S_j, S_{j+32}) ($j = 1, \ldots, J$; $J \leq 8$) where both signals were above the noise limit was determined. From those echo pairs, the signal intensity ratios Q_{meas_j} were computed. Each Q_{meas_j} corresponded to an individual T_{1_j} value which was equivalent to the LUT index with the best agreement between Q_{meas_j} and Q_{th}. In order to minimize the time needed to find the optimal index, a binary line-search algorithm was used, with a time complexity of $O(\log p)$ [55] where p is the number of LUT indices. Therefore, the optimal value was found after 12 scanning steps, at maximum. Because the signal strength and, therefore, the S/N decreases with increasing echo time due to the underlying T_2 relaxation process, each individual T_{1_j} was weighted with a factor f_{var_j} being inversely proportional to the variance in each estimate [29]:

$$f_{\text{var}_j} \equiv \frac{\sum_{k=1}^{K} \alpha_k \exp(-2\text{TE}_j/T_{2_k})}{\sum_{j=1}^{J}\sum_{k=1}^{K} \alpha_k \exp(-2\text{TE}_j/T_{2_k})} \quad (j = 1, \ldots, J; J \leq 8) \tag{8}$$

The measured T_1 was obtained from the weighted average of the individual T_{1_j} [27]:

$$T_1 = \sum_{j=1}^{J} f_{\text{var}_j} T_{1_j} \tag{9}$$

Finally, it was checked whether the result falls within the T_1 range 30–3000 ms, which was regarded as physiologically meaningful.

Knowing TR_1 and S_0 of the first echo train and T_1, the relative proton density ρ was obtained:

$$c\rho = \frac{\sum_{k=1}^{K} S_{0_k}(\text{TR}_1)}{1 - f_{SR_1}\exp(-\text{TR}_1/T_1)} \tag{10}$$

Normalization to a phantom substance of known water content (or any reproducibly measurable tissue) led to interexperimentally comparable ρ values.

RESULTS AND DISCUSSION

The phantom substances covered the whole physiological range of values: 300–2500 ms (T_1), 50–250 ms (T_2), and 75–100% (ρ). Relaxation behavior was exclusively monoexponential. Due to the extremely high S/N of the spectroscopy measurements, errors of the reference data were estimated to be 2%.

The results of the phantom measurements are presented in Fig. 3: up to T_1 = 2000 ms, the proposed imaging technique allowed to evaluate the longitudinal relaxation time without systematic errors, when compared to the spectroscopic reference data (Fig. 3, left). At even higher values of T_1, an underestimation was observed. This is considered of minor practical importance because extremely long relaxation times are observed only in fluids, where flow effects disturb the accuracy of the results anyhow. In general, the proposed technique suffers from the disadvantage that deviations of the excitation pulse angle from the ideal 90° have a rather strong effect on the accuracy, which cannot be corrected algorithmically due to the complexity of the resulting formulas and the small number of data points [37]. Choosing rather long TR_2 values minimizes this problem [37], but at the expense of a smaller number of theoretically measurable slices. With respect to TR_1 = 3000 ms, reproducibility may be improved slightly using longer TR_1 values [37], but this leads to higher measurement times. A high number of phantom experiments and simulations revealed that the combination TR_1 = 3000 ms/TR_2 = 600 ms represents a good compromise between accuracy, reproducibility and practicability [37].

Up to T_2 = 150 ms, the transverse relaxation time was evaluated systematically too high in the imaging data with a nearly constant offset over the observed T_2 range. This is explained by the strategy for trimming of the sequence (see above): Because trimming points were optimized only up to the third echo, later echoes potentially suffered contamination from stimulated echoes. This led to the relative contribution of higher-order echoes increasing with the number of transmitted RF pulses, i.e., at long TE times. As expected [56] T_2 was slightly overestimated (Fig. 3, center). It is concluded that the actual RF pulse profile (Gaussian shape) should be replaced by a better suited profile offering a better slice definition and causing less stimulated echoes. Furthermore, alternative trimming strategies to completely suppress stimulated echoes might be considered [57]. Very long T_2 times were underestimated, which is due to the rather fluid consistency of these samples and, therefore, to the significant influence of diffusion effects [37]. Again, it might be argued that tissues exhibiting T_2 values above 200 ms are very likely to be influenced by flow and perfusion effects.

Determination of the proton density ρ did not exhibit systematic errors, although overall accuracy was rather poor and the scatter was much higher than

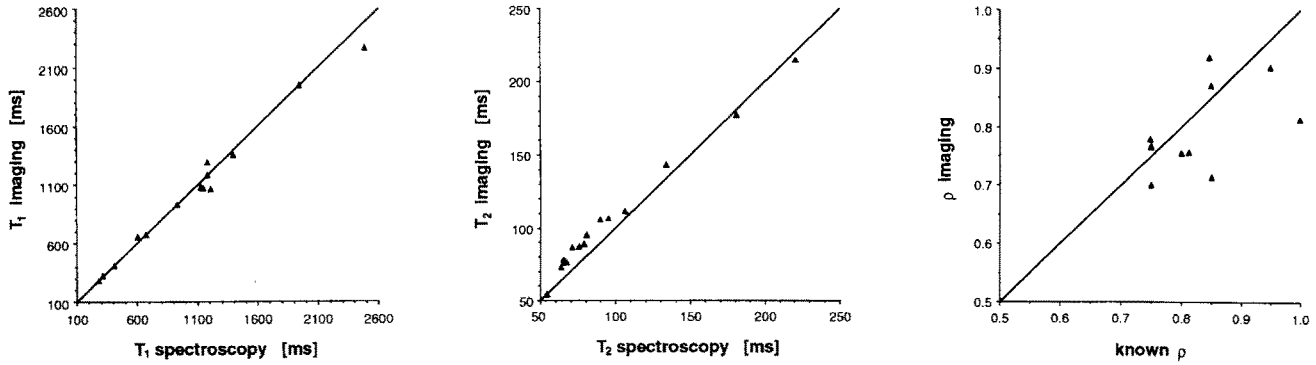

Fig. 3. Results of the phantom study. Comparison of the imaging results and of the measurements with the spectroscopy sequences (T_1, T_2) or the known ^1H content of the samples (ρ), respectively. The solid line represents the line of identity. Left (T_1): The range usually observed *in vivo* is evaluated with high accuracy (TR_1 = 4000 ms, TR_2 = 700 ms). Center (T_2): Over the range observed *in vivo*, T_2 times are slightly overestimated with the imaging sequence because of the trimming procedure used. Nevertheless, the absolute error remains nearly constant. Right (ρ): Overall accuracy was rather poor in comparison with the relaxation time measurements. The rather large scatter is thought to be due to problems during the preparation of the phantom substances.

that of the relaxation times (Fig. 3, right). This is thought to be due to the preparation of the substances: As the vials were not closed hermetically during heating of the mixture nor was the escaping vapor reliquified, a slight difference of the actually achieved proton densities from the desired ones could not be excluded.

The automatic algorithm for data preprocessing allowed the determination of the background noise within each image in a fast and reliable manner. Furthermore, effects of changing noise within the echo train was taken into account. In contrast to experimental studies, where movements of the measured "object" are significantly reduced due to the anesthesia of the animals and positioning in stereotaxic holders, this effect is especially observed in clinical investigations [29, 52]. In general, the preprocessing eliminated calculation of systematically wrong parameter values due to noise, especially for short T_2 times.

The use of an improved Marquardt algorithm [31, 32] for multiexponential T_2 analysis and of the described algorithm for T_1 determination allowed for the evaluation of high-quality relaxation parameter images with high spatial resolution (Fig. 4). Figure 4 shows the whole set of evaluated parameter images for two slices, measured in the study of experimental infarcts in rat brain.

So far, for detection of multiexponential T_2 decays, there are no alternatives to multiple echo sequences. The high number of acquired echoes can be utilized for nonlinear regression analysis only in the case of sufficient S/N. Due to the elevated T_1 times at high fields (1000–1300 ms in solid rat brain tissues at 4.7 T [37, 58], but only 600–1000 ms in healthy human brain at 1.5 T [31, 54], recovery times must be chosen according to the field strength of the imager. A value about three times the average T_1 must be regarded as sensible, indicating the generally long measurement times in quantitative T_2 imaging. For our *in vivo* studies at 4.7 T [37, 58], we used TR_1 = 3000 ms/TR_2 = 600 ms, twofold signal averaging and a 256 × 128 image matrix, which resulted in a measurement time of 17 min. The combination TR_1 = 2000 ms/TR_2 = 500 ms, an adequate choice at 1.5 T [31, 54], equals 12 min experimental time. With respect to the information content delivered by the sequence, this experimental time appears to be tolerable even in clinical routine [54]. Further substantial scan-time reduction might be achieved using a reduced number of phase-encoding steps (i.e., a 256 × 64 matrix), excessive zero filling, and retrospective removal of Gibbs ringing artifacts [59]. In contrast to independent sequences for the separate measurements of T_1 and T_2 [22–24, 26, 27, 36], the proposed method offers inherently perfect alignment of the three-dimensional parameter information contained in each pixel, which is extremely important for automatic tissue characterization approaches [60–63].

Computation time needed for evaluation of a parameter image depends both on the object size and on the number of biexponential pixels found. In the case of a coronal slice image of a rat (256^2; field of view 5 cm), the CPU requirements for a multiexponentially analyzed T_2 image amounts to 20 min on a VAXStation 3200 (Digital Equipment Corporation, Maynard, MA).

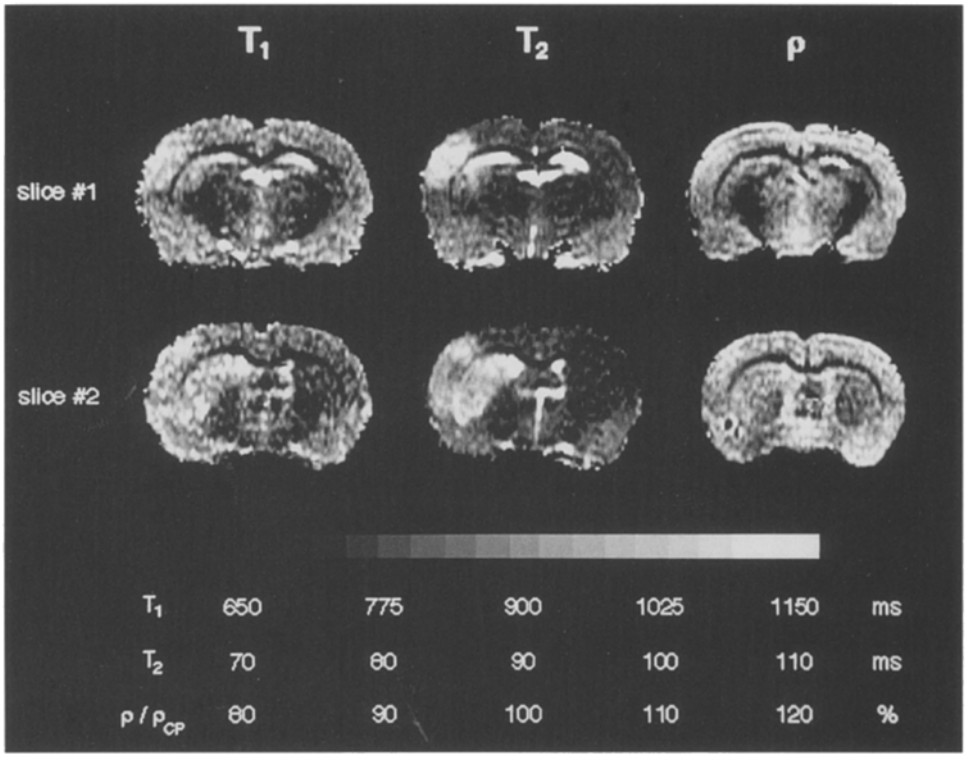

Fig. 4. Two coronal slices of calculated T_1, T_2 and ρ parameter images of a rat brain. The data was measured at 6 h after occlusion of the middle cerebral artery, taken from a study of experimental infarct in rat brain. Measurement parameters were TR_1/TR_2: 3000/600 ms; field of view 5.0 cm; slice thickness 1 mm; two averages; image matrix 128 × 256. Several structural details like differences between cortex and striatum are noted in both T_1 and ρ images. Ventricles have the longest relaxation times. Also, the white matter, seen as dark double arc in all three types of parameter images, is distinguished from gray matter due to its lower relaxation times and lower water content (reflected in a reduction of ρ). Clearly visible is the lesioned region in both T_1 and T_2 images as the area of elevated relaxation time in the left cortex and caudate putamen (CP). Note that the values of ^{1}H proton density ρ are normalized to that of the caudate putamen.

The consequent utilization of the information delivered by the T_2 analysis and the use of the weighted ratio algorithm allowed to compute high S/N T_1 images (Fig. 4). Thanks to the very fast LUT scanning technique, only about 20 s are needed for the generation of both T_1 and ρ image (parameters as above!). With more powerful computers, an on-line evaluation of the parameter images becomes possible, thus allowing the parameter images to be used directly for diagnosis.

CONCLUSIONS

In combination with the presented evaluation concepts, the imaging sequence was shown to allow the quantitatively correct measurement of T_1, T_2 and ρ. The simultaneous acquisition of all data, necessary for the complete description of the relaxation properties of each pixel, resulted in an efficient use of the measurement time. This makes the method attractive for clinical routine where investigation time must be minimized. The proposed sequence runs like any ordinary multiecho sequence, without compromise to practical versatility (e.g., multislice imaging, oblique slices) and without requirement of special adjustment procedures. In contrast to already reported sequences for simultaneous acquisition of T_1, T_2 (monoexponential) and ρ [6, 18, 28], which must be run as single slice experiments in practice, normally (choosing a moderate TR_1 time) three slices are possible with our sequence. Furthermore, due to the use of only two different recovery delays for collecting the T_1-sensitive information, the presented method runs considerably faster than other approaches [6, 18, 28]. Evaluation of T_1 based on the weighted average of several signal intensity ratios was already shown [29] to be less sensitive to image noise than the ordinary technique using the signal intensities of only two echoes [7, 11]. The use of the actual T_2 value for each pixel, shorten-

ing of the echo times, the extension to eight ratios, and consideration of the image background noise allowed further improvement of Riederer's approach [29] (one constant T_2 for weighting of all pixels; TE = 20 ms; four ratios; no noise processing). Additionally, the acquisition of a train of 32 echoes offers sufficient accuracy to perform multiexponential T_2 analysis. Since biexponential T_2 behavior was found in several tissues [5, 7, 9, 31, 51–54], this feature extends the potential of relaxometric investigations considerably and might lead to an improved specificity.

Furthermore, the chosen evaluation algorithms and the noise preprocessing guarantee short computation times. Using the latest, very powerful computer technology, an on-line computation of the parameter images should be expected. Therefore, the multidimensional MR parameter information contained in each pixel could be used directly for diagnosis. Additionally, this information can be analyzed and visualized further: Using image processing algorithms, cluster analysis, a tissue database and classification methods, the automatic differentiation and classification of tissues become possible [29, 54, 60–63].

ACKNOWLEDGMENTS

Stimulating discussions with Dr. H. Handels (Medizinische Universität Lübeck, Germany) and the technical assistance of H. Driessen (Rheinisch-Westfälische Technische Hochschule Aachen, Germany) are gratefully acknowledged. Further, we are grateful to Dr. T. Back for help with the animal experiment. This project was funded in part by a grant from the Deutsche Forschungsgemeinschaft (SFB 194/B1).

REFERENCES

1. Damadian R (1971) Tumor detection by nuclear magnetic resonance. *Science* **171:** 1151–1153.
2. Bottomley PA, Foster TH, Argersinger RE, Pfeifer LM (1984) A review of normal tissue hydrogen NMR relaxation times and relaxation mechanisms from 1–100 MHz: dependence on tissue type, NMR frequency, temperature, species, excision and age. *Med Phys* **11:** 425–448.
3. Beall PT, Amtey SR, Kasturi SR (1985) *NMR Data Handbook for Biomedical Applications.* New York: Pergamon Press.
4. Bottomley PA, Hardy CJ, Argersinger RE, Allen-Moore G (1987) A review of ^{1}H nuclear magnetic resonance relaxation in pathology: Are T_1 and T_2 diagnostic? *Med Phys* **14:** 1–37.
5. Gersonde K, Felsberg L, Tolxdorff T, Ratzel D, Ströbel B (1984) Analysis of multiple T_2 proton relaxation processes in human head and imaging on the basis of selective and assigned T_2 values. *Magn Reson Med* **1:** 463–477.
6. Just M, Higer HP, Schwarz M, Bohl J, Fries G, Pfannenstiel P, Thelen M (1988) Tissue characterization of benign brain tumors: Use of NMR tissue parameters. *Magn Reson Imaging* **6:** 463–472.
7. Schad LR, Brix G, Zuna I, Härle W, Lorenz WJ, Semmler W (1989) Multiexponential proton spin-spin relaxation in MR imaging of human brain tumors. *J Comp Assist Tomogr* **13:** 577–587.
8. Kjaer L, Thomsen C, Henriksen O (1989) Evaluation of biexponential relaxation behaviour in the human brain by magnetic resonance imaging. *Acta Radiol* **30:** 433–437.
9. Hoehn-Berlage M, Tolxdorff T, Bockhorst K, Okada Y, Ernestus R-I (1992) In vivo NMR T_2 relaxation of experimental brain tumors in the cat: A multiparameter tissue characterization. *Magn Reson Imaging* **10:** 935–947.
10. Pykett IL, Rosen BR, Buonanno FS, Brady TJ (1983) Measurement of spin-lattice relaxation times in nuclear magnetic resonance imaging. *Phys Med Biol* **28:** 723–729.
11. Lin MS (1984) Measurement of spin-lattice relaxation times in double spin-echo imaging. *Magn Reson Med* **1:** 361–369.
12. Kjos BO, Ehman RL, Brant-Zawadzki M (1985) Reproducibility of T_1 and T_2 relaxation times calculated from routine MR imaging sequences: Phantom study. *Am J Roentgenology* **144:** 1157–1163.
13. Redpath TW (1982) Calibration of the Aberdeen NMR imager for proton spin-lattice relaxation time measurements in vivo. *Phys Med Biol* **27:** 1057–1065.
14. Bydder GM, Young IR (1985) MRI: Clinical use of the inversion recovery sequence. *J Comp Assist Tomogr* **9:** 1020–1032.
15. Edelstein WA, Bottomley PA, Hart HR, Smith LS (1983) Signal, noise, and contrast in nuclear magnetic resonance (NMR) imaging. *J Comp Assist Tomogr* **7:** 391–401.
16. Kurland RJ (1985) Strategies and tactics in NMR imaging relaxation time measurements. I. Minimizing relaxation time errors due to image noise—the ideal case. *Magn Reson Med* **2:** 136–158.
17. Gowland PA, Leach MO, Sharp JC (1989) The use of an improved inversion pulse with the spin echo/inversion recovery sequence to give increased accuracy and reduced imaging time for T_1-measurements. *Magn Reson Med* **12:** 261–267.
18. Schneiders NJ, Ford JJ, Bryan RN (1985) Accurate T_1 and spin density NMR images. *Med Phys* **12:** 71–76.
19. Young IR, Hall AS, Bydder GM (1987) The design of a multiple inversion recovery sequence for T_1-measurement. *Magn Reson Med* **5:** 99–108.
20. Brix G, Schad LR, Deimling M, Lorenz WJ (1990) Fast and precise T_1 imaging using a TOMROP sequence. *Magn Reson Imaging* **8:** 351–356.
21. Crawley AP, Henkelman RM (1988) A comparison of one-shot and recovery methods in T_1-imaging. *Magn Reson Med* **7:** 23–34.
22. Haase A (1990) Snapshot FLASH MRI. Applications to T_1,

T_2, and chemical shift imaging. *Magn Reson Med* **13:** 77–89.
23. Haase A, Matthaei D, Bartkowski R, Dühmke E, Leibfritz D (1989) Inversion recovery snapshot FLASH MR imaging. *J Comp Assist Tomogr* **13:** 1036–1040.
24. Hoehn-Berlage M, Norris DG, Bockhorst K, Ernestus R-I Kloiber O, Bonnekoh P, Leibfritz D, Hossmann K-A (1992) T_1 snapshot FLASH measurement of rat brain glioma: Kinetics of the tumor-enhancing contrast agent Manganese(III) Tetraphenylporphine Sulfonate. *Magn Reson Med* **27:** 201–213.
25. Look DC and Locker DR (1970) Time saving in measurements of NMR and EPR relaxation times. *Rev Sci Instrum* **41:** 250–251.
26. Gowland PE, Mansfield P (1993) Accurate measurement of T_1 in vivo in less than 3 seconds using echo-planar imaging. *Magn Reson Med* **30:** 351–354.
27. Matthaei D, Haase A, Henrich D, Dühmke E (1992) Fast inversion recovery T_1 contrast and chemical shift contrast in high resolution snapshot FLASH MR images. *Magn Reson Imaging* **10:** 1–6.
28. Conturo TE, Price RR, Beth AH, Mitchell MR, Partain CL, James AE (1986) Improved determination of spin density, T_1 and T_2 from a three-parameter fit to multiple-delay–multiple-echo (MDME) NMR images. *Phys Med Biol* **31:** 1361–1380.
29. Riederer SJ, Bobman SA, Lee JN, Farzaneh F, Wang HZ (1986) Improved precision in calculated T_1 MR images using multiple spin-echo acquisition. *J Comp Assist Tomogr* **10:** 103–110.
30. Marquardt DW (1963) An algorithm for the estimation of non-linear parameters. *Soc Ind Appl Math J* **11:** 431–441.
31. Handels H (1992) *Automatische Analyse mehrdimensionaler Bilddaten zur Diagnoseunterstützung in der MR-Tomographie.* Aachen, Germany: Shaker.
32. Jostes C (1990) *Entwicklung und Implementierung eines Verfahrens zur Parameterschätzung bei multiexponentiellen T_2-Relaxationsprozessen in der MR-Tomographie.* Aachen, Germany: RWTH (Rheinisch Westfälische Technische Hochschule) Aachen (diploma thesis).
33. Conturo TE, Beth AH, Arenstorf RF, Price RR (1987) Simplified mathematical description of longitudinal recovery in multiple-echo sequences. *Magn Reson Med* **4:** 282–288.
34. Hahn EL (1950) Spin echoes. *Phys Rev* **80:** 580–594.
35. Carr HY, Purcell EM (1954) Effects of diffusion on free precession in NMR experiments. *Phys Rev* **94:** 630–638.
36. Meiboom S, Gill D (1958) Modified spin echo method for measuring nuclear relaxation times. *Rev Sci Instrum* **29:** 688–691.
37. Eis M (1993) *Entwicklung von Verfahren zur quantitativen Magnet-Resonanz-Bildgebung der Relaxation und Diffusion und deren Anwendung in der experimentellen Neurologie.* Aachen, Germany: Verlag Mainz.
38. Eis M, Hoehn-Berlage M, Bockhorst K, Hossmann K-A (1991) A time efficient method for combined T_1/T_2 relaxation time measurements. Evaluation for multiparameter tissue characterization. In *Book of Abstracts of the 10th Annual Meeting of the Society of Magnetic Resonance in Medicine* (Society of Magnetic Resonance in Medicine eds) Berkeley, CA p. 701.
39. Kraft KA, Fatouros PP, Clarke GD, Kishore PRS (1987) A MRI phantom material for quantitative relaxometry. *Magn Reson Med* **5:** 555–562.
40. Santyr GE, Henkelman RM, Bronskill MJ (1988) Variation in measured transverse relaxation in tissue resulting from spin locking with the CPMG sequence. *J Magn Reson* **79:** 28–44.
41. James F, Roos M (1967/85) *MINUIT—Function minimization and error analysis.* Geneva: CERN Computer Centre (program library, utility D506).
42. Edelstein W, Glover G, Hardy C, Redington R (1986) The intrinsic signal-to-noise ratio in NMR imaging. *Magn Reson Med* **3:** 604–618.
43. Bellon EM, Haacke EM, Coleman PE, Sacco DC, Steiger DA, Gangarosa RE (1986) MR-artifacts: a review. *Am J Roentgenology* **147:** 1271–1281.
44. Edelstein W, Bottomley PA, Pfeifer LM (1984) A signal-to-noise calibration procedure for NMR imaging systems. *Med Phys* **11:** 180–185.
45. Henkelman RM (1985) Measurement of signal intensities in the presence of noise in MR images. *Med Phys* **12:** 232–233.
46. Handels H, Tolxdorff T, Bohndorf K (1990) Preprocessing of magnetization decays to improve multiexponential T_2 analysis. In *Tissue Characterization in MR Imaging* (Higer H-P and Bielke G, eds) pp. 69–74. Berlin: Springer-Verlag
47. Barroilhet LE, Moran PR (1975) Nuclear magnetic resonance (NMR) relaxation spectroscopy in tissues. *Med Phys* **2:** 191–194.
48. Chang DC, Hazlewood CF, Woessner DE (1976) The spin-lattice relaxation times of water associated with early post mortem changes in skeletal muscle. *Biochim Biophys Acta* **437:** 253–258.
49. Sandhu HS, Friedmann GB (1978) Proton spin-lattice relaxation time study in tissues of the adult newt Taricha granulosa (Amphibia: Urodele). *Med Phys* **5:** 514–517.
50. Bakker CJG, Vriend J (1984) Multiexponential water proton spin-lattice relaxation in biological tissues and its implications for quantitative NMR imaging. *Phys Med Biol* **29:** 509–518.
51. Barthwal R, Hoehn-Berlage M, Gersonde K (1986) In vitro proton T_1 and T_2 studies on rat liver: Analysis of multiexponential relaxation processes. *Magn Reson Med* **3:** 836–875.
52. Kamman RL, Bakker CJG, van Dijk P, Stomp GP, Heiner AP, Berendsen HJC (1987) Multiexponential relaxation analysis with MRI and NMR spectroscopy using fat-water systems. *Magn Reson Imag* **5:** 381–392.
53. Armspach JP, Gounot D, Rumbach L, Chambron J (1991) In vivo determination of multiexponential T_2 relaxation in the brain of patients with multiple sclerosis. *Magn Reson Imaging* **9:** 107–113.
54. Reul J, Handels H, Thron A, Lakenberg C, Herpers R (1992) Relaxometrische Differenzierung normaler und

pathologischer Hirngewebe in der MR-Tomographie unter Verwendung einer histogrammbasierten Cluster-Analyse. *Klin Neuroradiol* **2:** 55–63.
55. Wirth N (1979) *Algorithmen und Datenstrukturen.* Stuttgart: Teubner.
56. Majumdar S, Orphanoudakis SC, Gmitro A, O'Donnell M, Gore JC (1986) Errors in the measurement of T_2 using multiple-echo MRI-techniques. I: Effects of RF pulse imperfections. *Magn Reson Med* **3:** 397–417.
57. Crawley AP, Henkelman RM (1986) Suppression of stimulated echoes in multislice T_2 imaging. In *Book of Abstracts of the 5th Annual Meeting of the Society of Magnetic Resonance in Medicine* (Society of Magnetic Resonance in Medicine eds) Berkeley, CA pp. 1061–1062.
58. Wilmes LJ, Hoehn-Berlage M, Els T, Bockhorst K, Eis M, Bonnekoh P, Hossmann K-A (1993) In vivo relaxometry of three brain tumors in the rat: Effect of Mn-TPPS, a tumor-selective contrast agent. *Journal of Magnetic Resonance Imaging* **3:** 5–12.
59. Constable RT, Henkelman RM (1991) Data extrapolation for truncation artifact removal. *Magn Reson Med* **17:** 108–118.
60. Handels H, Tolxdorff T (1990) A new segmentation algorithm for knowledge acquisition in tissue characterizing NMR imaging. *J Digit Imaging* **3:** 89–94.
61. Handels H, Hiestermann A, Tolxdorff T, Thron A, Bohndorf K, Eis M (1990) Automatic segmentation of tissue in 3D voxel space based on multidimensional MR parameter histograms. In *Book of Abstracts of the 9th Annual Meeting of the Society of Magnetic Resonance in Medicine* (Society of Magnetic Resonance in Medicine eds) Berkeley, CA p. 556.
62. Handels H (1993) Automatic segmentation and classification of multiparametric image data in medicine. In *Studies in Classification, Data Analysis and Knowledge Organization.* (Klar R, Lausen B, Opitz O, eds). pp. 452–460 Berlin: Springer-Verlag.
63. Eis M, Handels H, Hoehn-Berlage M, Wilmes LJ, Ernestus R-I, Kloiber O, Tolxdorff T, Hossmann K-A (1991) Fully automatic tissue characterization in rat brain at 4.7 T. In *Book of Abstracts of the 10th Annual Meeting of the Society of Magnetic Resonance in Medicine* (Society of Magnetic Resonance in Medicine eds) Berkeley, CA p. 1214.